Simulations of amperometric monitoring of exocytosis: moderate pH variations within the cell-electrode cleft with the buffer diffusion

Yann Bouret, Manon Guille-Collignon, Frédéric Lemaître

Simulations of Amperometric Monitoring of Exocytosis: Moderate pH Variations within the Cell-Electrode Cleft with the Buffer Diffusion

Yann Bouret,[a] Manon Guille-Collignon,[b] Frédéric Lemaître[b,*]

[a] *Université Nice Côte d'Azur, CNRS-UMR 7010 Institut de Physique de Nice, Av. Joseph Vallot, 06100 NICE*

[b] *PASTEUR, Département de chimie, École normale supérieure, PSL University, Sorbonne Université, CNRS, 75005 Paris, France*

* *corresponding author: frederic.lemaitre@ens.psl.eu*

Keywords: vesicular exocytosis, amperometry, ultramicroelectrodes, pH, simulations

Abstract

Amperometry with ultramicroelectrodes is nowadays a routine technique to investigate neurotransmitter secretion by vesicular exocytosis at the single cell level. This electroanalytical tool allows one to understand many aspects of the vesicular release in terms of mechanisms. However, the electrochemical detection relies on the oxidation of released neurotransmitters that produces $2H^+$ and thus the possible acidification of the cell-electrode cleft. In a previous work, we considered a model involving the H^+ diffusion or/and its reaction with buffer species. In this article, we report a more general model which takes into account the ability of buffer species to move and to be regenerated within the cell-electrode cleft. As a consequence, the pH within the cleft is still equal to its physiological value regardless of the electrochemical detection of the vesicular release for usual exocytotic cell frequencies. This confirms that amperometry at the single cell level is a very robust technique for investigating vesicular exocytosis.

Introduction

Vesicular exocytosis is probably one of the most fascinating mechanisms involved in Biology. This important pathway of communication (neurotransmission, hormone release) is based on the ability for the emitting cell to release biomolecules (neurotransmitters or hormones) from the intracellular medium to the extracellular solution whereas the cell membrane is not permeable to such molecular structures.[1-3] To do so, neurotransmitters are initially packed within vesicles that fuse with the cell membrane. This leads to a transient nanometric fusion pore through which the release begins. Its evolution strongly depends on the cell model and the vesicular content and the fusion pore can either close or expand to a partial or full release (**Figure 1**).

Actually, the main steps are globally figured out but the main biophysical parameters that govern the mechanism and especially its plasticity remain under debate. In that respect, amperometry with an ultramicroelectrode (UME) at the single cell level was implemented to monitor exocytosis in real time forty years ago.[4,5] The experimental principle is to oxidize the released species by the emitting cell at the electrode surface. Each vesicular event is individually displayed as an amperometric spike (**Figure 1**) featuring the release in terms of kinetics (current magnitude, time length) and amount of detected neurotransmitters (spike area).[6-8] This analytical tool has fundamentally changed the way to investigate exocytosis because it allows one to finely study how modifications of a given parameter (extracellular ionic composition, cell membrane properties like viscosity or curvature, protein assemblies…) play a key role on the ability for the cell to perform exocytosis.[6, 9] It also significantly contributes to the issues related to the mode of release[10-12] and calculations of the final opening angle for a given vesicular event.[13] To date, amperometry with UMEs has become an indispensable tool to a wide range of researchers (chemists, biophysicists, and biologists) who use it as a routine technique as an important complementary tool of fluorescence[14-17] and electrophysiological techniques.[18] Recent developments evidence that this electroanalytical tool can be even used for intracellular analyses[7,12,16,19] or within a real synapse with nanoelectrodes.[20-22]

Nevertheless, such a technique may lead to serious analytical biases that would make it less reliable as expected. A first one is related to superimposition between subsequent events that can make the analysis misleading. This issue was solved ten years ago and led to important criteria to respect for a proper analysis.[23,24] The second one concerns the pH within the cell-electrode cleft. Indeed, the oxidation of usual neurotransmitters (catecholamines e.g. adrenaline, dopamine…) involves a $2e^-/2H^+$ pathway that may drastically increase the acidity of the physiological solution between the emitting cell and the collecting electrode (**Figure 2**). Low pH values close to the investigated cell could alter the cell functions and therefore its ability to release biomolecules by vesicular

exocytosis. In other words, the amperometric detection could bias itself by modifying the biological organism. This question is important for the technique itself and even more so as it is coupled to fluorescence monitoring with pH-dependent fluorescent probes.[25-28]

This issue was addressed in a previous theoretical work confirming that the electrochemically induced acidification should occur and depends on the electrode size as well as the exocytotic frequency.[29] However, such results were sometimes inconsistent with experimental results evidencing that the electrode surface area did not modify the amperometric spikes features. In this paper, we report on a fundamental modification of this previous model that now takes into account the diffusion of the buffer and its ability to be replenished with the cell-electrode cleft with its diffusion. By taking into account this important parameter, we showed that the induced pH variations within the cell-electrode cleft are moderate and compatible with a non invasive electrochemical technique.

Results and discussion

1. Addressing a proton only diffusion in a reactive cleft

This is the initial view we previously reported elsewhere.[29] The cell-electrode cleft is a very thin cylindrical film (radius "r"; height "h"; see **Figure 2**) of aqueous solution connected to the extracellular buffer only by its submicrometric edge (r ~ µm; h = 100 nm). The model relied on the two pathways of electrogenerated H^+ by the electrochemical detection of catecholamines. First, they may be neutralized by the buffer inside the cleft. Second, they may diffuse towards the extracellular medium. Of note, non-electrochemically generated protons are also released from the intravesicular medium (vesicular pH being 5.5) but their maximum amount is considerably less than that of those induced by amperometry (intravesicular concentration of catecholamines ~ 0.6 mol.L^{-1}; intravesicular concentration of protons = $10^{-5.5}$ ~ 3×10^{-6} mol L^{-1}).

Briefly, in a Cartesian coordinate system, since h << r, diffusion across the "z" axis may be averaged and the proton concentration therefore depends on the coordinates "x" and "y". The diffusing proton concentration "C" for each vertical position ($0 \le z \le h$) is thus defined according to (equation (1)):

$$C(x,y,t) = \frac{1}{h}\int_0^h [\mathrm{H}^+](x,y,z,t)dz \quad (1)$$

As a consequence, the proton concentration related to diffusion within the clefts obeys to Fick's second law according to equation (2):

$$\frac{\partial C}{\partial t} = D\left(\frac{\partial^2 C}{\partial x^2} + \frac{\partial^2 C}{\partial y^2}\right) \quad (2)$$

The proton diffusion coefficient "D" value corresponds to its autodiffusion in aqueous medium.

Moreover, from a chemical point of view, two acid-base reactions need to be also considered for the aqueous solution within the cell-electrode cleft (H_3O^+ is noted H^+ for simplification), i.e. self-ionization of water (equation (3)) and equilibrium involving the buffer used for maintaining the pH solution at 7.4 (AH/A^- couple; equation (4)). Both reactions (that are fast enough to still be at equilibrium at any pH that is reached) take place within the cleft according to:

$$H_2O \rightleftharpoons OH^- + H^+ \qquad (K_w) \qquad (3)$$

$$AH \rightleftharpoons A^- + H^+ \qquad (K_a) \qquad (4)$$

We firstly assumed that those simple reactions were always at equilibrium, meaning that after a chemically uncoupled diffusive step to solve equation (2) (using a Crank-Nicholson finite difference scheme on a uniform 2D-space grid and uniform time grid), an instantaneous chemical step is applied to compute the new equilibria (3) and (4) throughout the whole simulation space. A more detailed discussion of these assumptions and of these methods is discussed below, according to more recent developments.

Moreover, the two following boundary conditions were also applied at the end of the cleft:

$$t \geq 0,\ \sqrt{x^2 + y^2} = r \Leftrightarrow C = 10^{-\mathrm{pH}_{buffer}} \qquad (5)$$

$$t = 0,\ \sqrt{x^2 + y^2} \leq r \Leftrightarrow C = 10^{-\mathrm{pH}_{buffer}} \qquad (6)$$

The catecholamine release (including their diffusion over the "h" distance and their electrochemical oxidation) is fast enough to be converted into a sudden and localized proton bursts. In this respect, flash H^+ sources are delivered in a small volume which is related to the vesicular radius (r_{Ves} = 150 nm). Therefore, the sequence of proton sources is randomly distributed at different positions over the cleft surface at a global frequency F. This parameter is related to usual exocytotic frequencies measured by amperometry and can be adjusted according to $F = F_s \pi r^2$ (with F in Hz and r in µm). F_s is the surfacic exocytotic frequency which is equal to 0.026 $Hz.\mu m^{-2}$. Such a surfacic frequency value remains constant for all simulations but leads to different exocytotic frequencies depending on the electrode radius. Of note, this corresponds to the range of usual experimental frequencies (F = 2 Hz for r = 5 µm).

Finally, other parameters are fixed. Simulations are obtained for a physiological situation during the measurements, i.e. when HEPES buffer (pKa = 7.5) is used (10 mmol.L^{-1}) at pH_{buffer} = 7.4. The electrochemical oxidation of catecholamines releases two protons from an intravesicular concentration equal to 0.6 mol.L^{-1}. The diffusion coefficients for H^+ and OH^- were taken from their values in water, i.e. 9.3x10^{-9} and 5.3x10^{-9} m^2.s^{-1} respectively. *Of note, the buffer species diffusion was not considered* due to their relatively low value (5x10^{-10} m^2.s^{-1})[30, 31] compared to the corresponding proton value.

From the proton concentrations resulting from the numerical simulations, one can define the mean pH within the cleft (for pH values ranging from 5 to 7, activity coefficients close to unity are neglected) as:

$$pH_{mean} = -\log\left(\frac{\iint_{cleft} C dx dy}{\pi r^2}\right) \quad (7)$$

A typical pH = f(t) curve is depicted in **Figure 3** for r = 5 µm and F = 2 Hz. Each isolated H^+ bursts are progressively compensated by reaction-diffusion pathways (**Figure 2)** but the relaxing pH appears as more acidic than the buffered value (i.e. pH 7.4). This is consistent with a titration of the electrogenerated protons by the motionless buffer within the cleft.

Under such conditions, the mean pH rapidly becomes constant and reaches a relaxation pH equal to 6.65, an acidic pH raising questions about the possible effects towards the cell integrity or even the electrochemical detection itself whose mechanism is pH-dependent.[32-37] The fact that experimental results evidenced no effects of the electrode radius on the measured currents suggests that this model did not take into account all the relevant parameters.[23, 29] This is why we consider a new approach including the buffer diffusion.

2. Accounting for a fully diffusive cleft

2.1. Description and framework

2.1.1. Basic assumptions

In a first approach, we considered that the diffusion process was essentially driven by the sole diffusion of H^+ with respect to its greatest diffusion coefficient. Nonetheless, the other species are still diffusing and hence (i) may escape from the cleft when they are created within or (ii) on the contrary may be renewed through the boundaries conditions. Consequently, since all the considered species posses similar diffusion coefficients (see above), we need to take them all into account to investigate these effects.

Furthermore, in such a medium, the ionic strength is considered as high enough to only allow the autodiffusion of each ionic species, i.e. without further electrostatic coupling. Therefore, each species S follows the second Fick's law with its diffusion coefficient D_S (equation (8)) and are constrained by the set-up geometrical boundary conditions (see above):

$$\frac{\partial[S]}{\partial t} = D_S \Delta[S] \quad (8)$$

Additionally, each species may be involved in one or many chemical reactions that classically add optional source terms in equation (8). These basic assumptions are coherent and uniform with the first version of the model.

2.1.2 Chemical timescales

The acid-base reactions involving water and buffer dissociations are still considered (equations (3) and (4)) like in the previous model. The relaxation time for water self-dissociation is around a microsecond, and this is the characteristic time-scale for about all protic equilibria. Physiologically, this fast relaxation times allows one to consider some "slower" reactions (mostly membrane transport of protic species) as a perturbation of all the protic equilibria. A short review of these time scales and a way to derive the proper kinetic equations in such a case were derived in reference [38] and furthermore applied in reference [39].

2.1.3. Diffusive timescales

As mentioned above, we considered usual diffusion coefficient values for H^+ and OH^- (i.e. 9.3×10^{-9} and 5.3×10^{-9} $m^2.s^{-1}$ respectively) in water. Values for buffer species (AH and A^-) were taken as equal to 5×10^{-10} $m^2.s^{-1}$.[30,31] Here, the fastest diffusive species is the proton, according to both its size and the hydrogen bond dynamics. Consequently, a simple estimation points out that for length scales above a few nanometers, the diffusion is a perturbation of all the protic equilibria. Hence, we will use here an adapted version of the computational framework successfully harnessed in our previous works.[38,39]

2.2. Asymptotic diffusion

2.2.1. Specific chemical problem

We wish to simulate the diffusion in a space described by the vector "$\vec{r}(x,y)$" and as a function of time "t" of four species, H^+, OH^-, AH and A^- (see above), starting from an equilibrium state where the following conditions are satisfied everywhere from equations (3) and (4):

$$\begin{cases} 0 = K_W - [H^+][\mathrm{OH}^-] \\ 0 = K_a[AH] - [H^+][A^-] \end{cases} \quad (9)$$

As a consequence, one can define the vector of concentrations according to:

$$\vec{C} = \begin{pmatrix} [H^+] \\ [OH^-] \\ [\mathrm{AH}] \\ [\mathrm{A}^-] \end{pmatrix} \quad (10)$$

The extent matrix and the Jacobian matrix of equation (9) are thus:

$$\nu = \begin{pmatrix} 1 & 1 & 0 & 0 \\ 1 & 0 & -1 & 1 \end{pmatrix} \quad (11)$$

$$J = \begin{pmatrix} -[OH^-] & -[H^+] & 0 & 0 \\ -[\mathrm{A}^-] & 0 & K_a & -[H^+] \end{pmatrix} \quad (12)$$

2.2.2. Specific diffusion problem

As mentioned above, the diffusion of the four species follows the second Fick's law according to:

$$\begin{cases} \dfrac{\partial [H^+]}{\partial t} = D_{H^+} \Delta [H^+] \\ \dfrac{\partial [OH^-]}{\partial t} = D_{OH^-} \Delta [OH^-] \\ \dfrac{\partial [AH]}{\partial t} = D_{AH} \Delta [AH] \\ \dfrac{\partial [A^-]}{\partial t} = D_{A^-} \Delta [A^-] \end{cases} \quad (13)$$

Once the boundary conditions are chosen, an alternating-direction Crank-Nicolson scheme is implemented to obtain the diffusional increase $\delta\vec{C}(\vec{r},t)$ at each chosen point in space, for a time-step δt, which is formally an operator L:

$$\delta \vec{C}(\vec{r},t) = L\left(\vec{C}(\vec{r},t), \delta t\right) \quad (14)$$

2.2.3. Specific chemical problem

Obviously, the unconstrained step $\delta\vec{C}$ sends the phase space out of the "legal" conditions defined by equation (9). As shown in previous works, the chemical system produces an instantaneous extent (namely very fast compared to the diffusive perturbation) which chemically modifies the concentrations to return to a new phase space that satisfies the constraints represented by equation (9). The constrained value is:

$$\delta_\chi \vec{C}(\vec{r},t) = \underbrace{\left[\boldsymbol{I} - {}^t\boldsymbol{J}(\boldsymbol{J}\,{}^t\nu)^{-1}\boldsymbol{J}\right]}_{of\ \vec{C}(\vec{r},t)} L\left(\vec{C}(\vec{r},t),\delta t\right) \tag{15}$$

Eventually, we define by equation (15) the modified diffusion step, *where an asymptotically fast relaxing system is driven by a perturbative diffusion*.

2.2.4. Chemical balance

From now on, the "asymptotic" values of the new concentrations can be computed according to:

$$\vec{C}_\chi(\vec{r},t+\delta t) = \vec{C}(\vec{r},t) + \left[\boldsymbol{I} - {}^t\boldsymbol{J}(\boldsymbol{J}\,{}^t\nu)^{-1}\boldsymbol{J}\right] L\left(\vec{C},\delta t\right) \tag{16}$$

But since the constraints defined by equation (10) are not linear, this expression is still not correct. We need to let the chemical system evolve to reach a valid state. This is numerically performed by a few Newton's steps: thanks to the asymptotic formulation, the guess concentration $\vec{C}_\chi(\vec{r},t+\delta t)$ is never too far from such a state, and generally only one or two Newton's steps are sufficient to reach a numerical result with a precision less than the computer floating point tolerance.

3. Results with the general model

3.1. Relaxation pH after H^+ pulses is related to the buffer motion

The first results from the new model are displayed in **Figure 4**. The electrochemical oxidation of catecholamines corresponds to a $2e^-/2H^+$ process. The pH buffer is 7.4 and the HEPES concentration is 10 mmol.L^{-1}. All the other relevant parameters are extracted from the usual chromaffin cell model.[40, 41] The initial neurotransmitter vesicular concentration is 0.6 mol L^{-1} and the mean vesicular radius is 150 nm. The cell-electrode cleft thickness is 100 nm and the exocytotic surface frequency is equal to 0.026 Hz.μm^{-2} thus leading to the mean observed value of 2 Hz for r = 5 µm. The used diffusion coefficients for HEPES, $HEPES^-$, OH^- and H^+ are described above. As displayed in **Figure 4** (for three electrode radii = 1, 5 and 10

μm), taking into account the buffer motion significantly modifies the pH variation within the cell-electrode cleft overtime. Indeed, with a motionless buffer, each H^+ pulse (due to the electrochemical detection) is partially compensated by the internal medium. The mean pH value initially decreases and rapidly reaches a constant value after each proton bursts. This results from competitive phenomena including the H^+ diffusion (due to a concentration gradient) from the cleft to the external medium and the H^+ reaction with the buffer (that is quickly overwhelmed within the cleft). As demonstrated with the old model, the more the electrode radius is, the less the relaxation pH value is. Conversely, by including the buffer motion in the model, the relaxation pH value remains equal to the external buffer value (i.e. 7.4), irrespective of the electrode radius. This means that the buffer motion is a key point to model such a system. More importantly, *this shows that the continuous buffer motion and its renewal are able to prevent a significant acidification of the cell vicinity due the electrochemical detection*. This is confirmed by further simulations where the constant relaxation pH value as a function of the electrode radius remains equal to 7.4 (**Figure 5**).

3.2. Supplementary simulations and analyses evidence the crucial role of the buffer

3.2.1. Complementary simulations

Beyond its property to move within the cleft, other crucial roles of the buffer are evidenced by supplementary simulations. As an example, both buffer forms are required as displayed in **Figure 6**. Only movable acidic or basic forms both prevent the pH to be restored at pH 7.4. Furthermore, increasing the buffer concentration from 10 to 100 mmol.L^{-1} did not change the relaxed pH (already equal to 7.4 for a movable buffer at 10 mmol.L^{-1}).

3.2.2. *Other analyzed parameters*

We mostly analyzed the results in terms of relaxed pH by comparison with the important physiological value. However, complementary data treatment can be achieved in terms of ability of the medium within the cleft to compensate the pH pulses. In this way, we chose to extract two new parameters: the maximum pH variation due to a pH pulse and the time duration for returning to the relaxed pH baseline (**Table 1**).

A first important result concerns the real experimental case, ie for r = 5 μm and a movable buffer at 10 mM. Indeed, the pH variation remains quite low (0.37 ± 0.08) and with a mean duration (57 ± 2) ms in the same range than the half-time width of a typical amperometric spike from a vesicular release from chromaffin cells.[40, 41] This means that the whole duration of an exocytotic event is significantly larger than the time period required for neutralizing the pH pulse thus reinforcing the fact that the electrochemical detection did not alter the investigated cell.

Of note, the ΔpH and Δt values are globally consistent with the other different simulations (**Table 1**). First of all, for a given electrode radius (r = 5 µm), motionless buffer forms drastically decrease the pH variations (1.24 ± 0.08) and the pulse duration (489 ± 1) ms. As expected for only one form in solution, the acidic and basic forms are both essential. Preventing the motion of the basic form expectedly leads to a significant acidification of the cleft as shown by the pH pulse values (4.98 ± 0.15). Allowing the basic form only to move results in lower pH pulses (1.05 ± 0.12) while the relaxed pH remains lower than 7.4.
Finally, increasing the (mobile) buffer concentration leads to almost prevent the acidification of the cleft (0.11 ± 0.02 and 38 ± 1 ms). It has to be emphasized that the electrode radius is still important. Because the H^+ diffusion is made easier for lower electrode dimensions, the electrochemical detection has no effect for r = 1 µm. Conversely, a higher radius (r = 10 µm) corresponds to higher pulses durations (108 ± 3) ms while pH variations remains statistically almost constant (0.17 ± 0.10) by comparison with the typical case (r = 5 µm).

Conclusion

In this paper, we showed that the pH values within the cell-electrode cleft remains close to the external buffer value during amperometric measurements of exocytosis in usual cell models (chromaffin cells, PC12…) and ultramicroelectrode sizes. The possible acidification resulting from the electrochemical detection of catecholamines is then prevented by the H^+ diffusion but especially by the motion of buffer whereas its diffusion is significantly lower. While acidification of investigated single cells could be deleterious, this confirms that the historically detection of exocytosis with ultramicroelectrodes is a reliable and non invasive electrochemical technique.

Acknowledgements

This work has been supported in part by CNRS (UMR 8640), Ecole Normale Supérieure, French Ministry of Research, Faculté des Sciences et Ingénierie - Sorbonne Université. M. G-C. thanks “Emergences Ville de Paris 2014” Grant and Institut Universitaire de France Junior 2015 Fellowship Program.

Tables

Table 1. pH pulses and time lengths for different electrode radii and buffer motions or concentrations

r (μm)	5	5	5	10	1
Buffer concentration (mM)	10	10	100	10	10
Movable buffer?	NO	YES	YES	YES	YES
ΔpH	1.24 ± 0.08	0.37 ± 0.08	0.11 ± 0.02	0.17 ± 0.10	0
Δt (ms)	489 ± 1	57 ± 2	38 ± 1	108 ± 3	-

Figure captions

Figure 1. Top: Experimental set-up for electrochemically monitoring vesicular exocytosis at the single cell level. Bottom: representative current spike recorded by amperometry and corresponding to the oxidation of released neurotransmitters. The pre-spike feature (PSF) results from the preliminary fusion pore step. The main spike defines the massive release. An event can be featured by kinetic (maximum current, half time width) and quantitative (area $\propto$ amount of detected neurotransmitters) parameters.

Figure 2. Top: Geometrical description of the reaction-diffusion scheme involving proton bursts within the cell-electrode cleft. Bottom: fates of the protons resulting from the electrochemical oxidation of the neurotransmitter catechol moiety. H^+ may diffuse due to the concentration gradient or react with the movable basic form of the buffer (ie HEPES).

Figure 3. Typical pH = f(t) simulations from the « old » model with a motionless buffer (r = 5 µm ; h = 100 nm ; F_S = 0.026 Hz.µm^{-2} ; $C_{neurotransmitters}$ = 0.6 mol.L^{-1}). The inset displays the relaxation pH and the ΔpH variations due to each detected vesicular event (see text).

Figure 4. pH simulations within the cleft (h = 100 nm ; F_S = 0.026 Hz.µm^{-2} ; $C_{neurotransmitters}$ = 0.6 mol.L^{-1}). Red curves correspond to the case where the AH/A$^-$ buffer is movable. Black curves correspond to the case where the AH/A$^-$ buffer is motionless. A) r = 5 µm. B) r = 1 µm. C) r = 10 µm.

Figure 5. Constant relaxation pH values (from simulations in Figure 4) as a function of the electrode radius for two cases: motionless AH/A$^-$ buffer (black) vs movable AH/A$^-$ buffer (red).

Figure 6. pH = f(t) simulations for some cases depending on the buffer parameters. Black: movable AH/A$^-$ buffer at 10 mmol.L^{-1}; Red: movable AH/A$^-$ buffer at 100 mmol.L^{-1}; Green: buffer at 10 mmol.L^{-1} with movable AH/motionless A$^-$; Blue: buffer at 10 mmol.L^{-1} with motionless AH/ movable A$^-$.

Figure 1

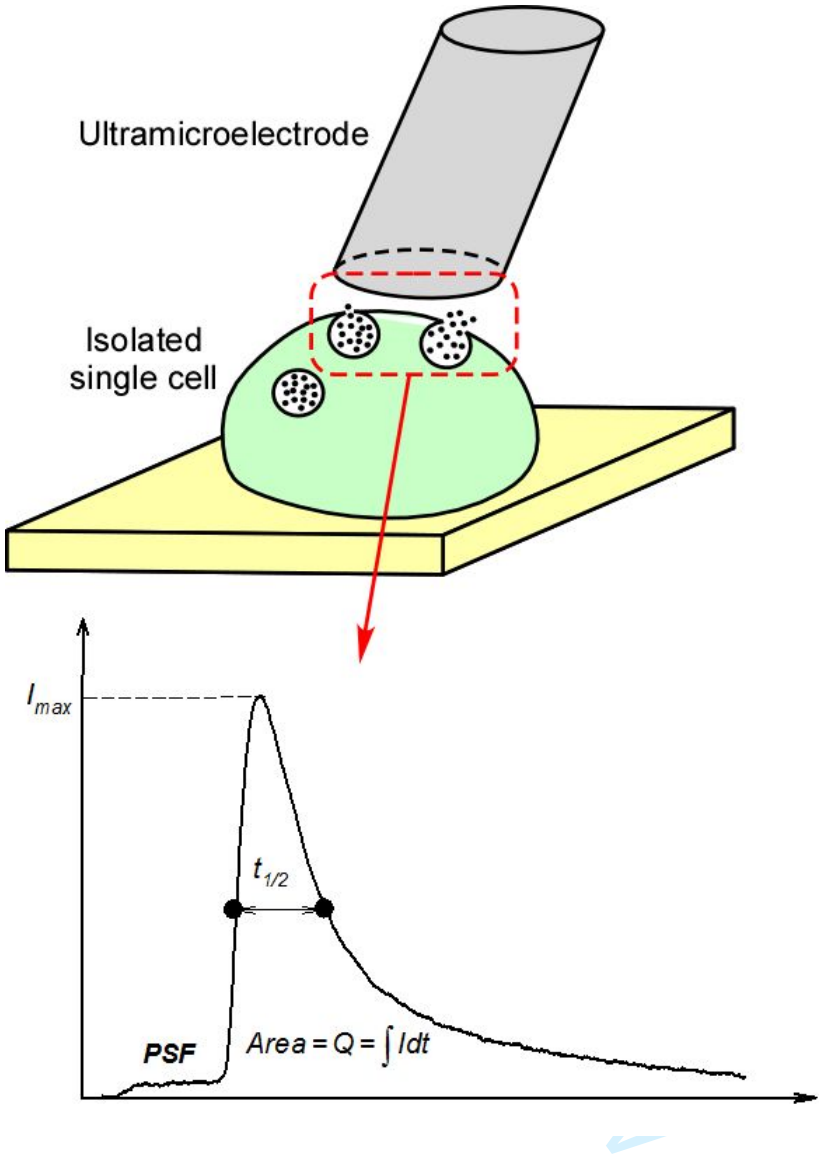
Ultramicroelectrode
Isolated
single cell
I_{max}
$t_{1/2}$
PSF
Area = Q = ∫ Idt

Figure 2

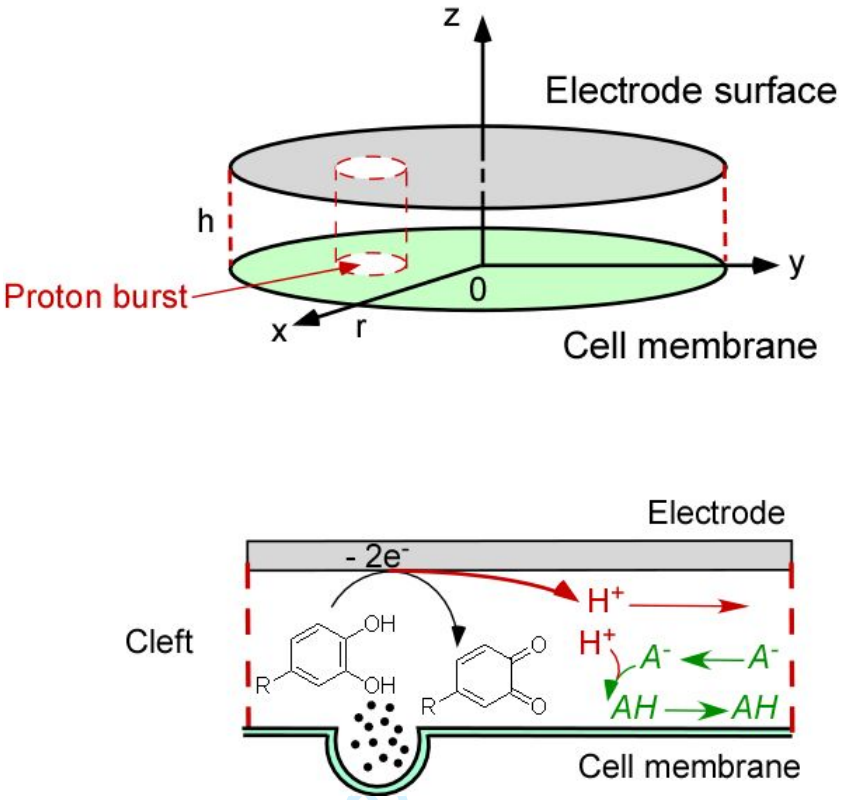

Figure 3

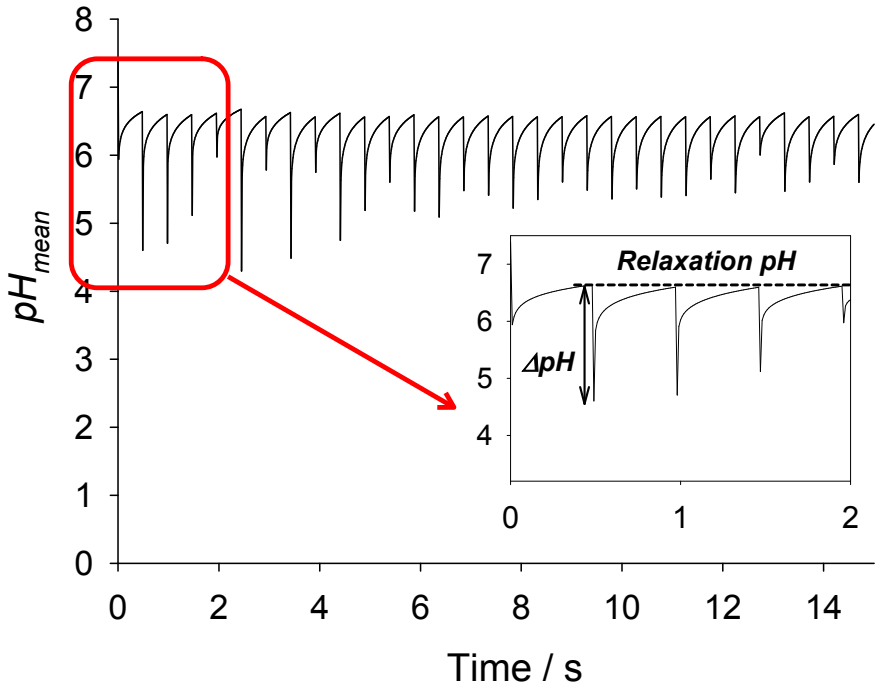

Figure 4

A)

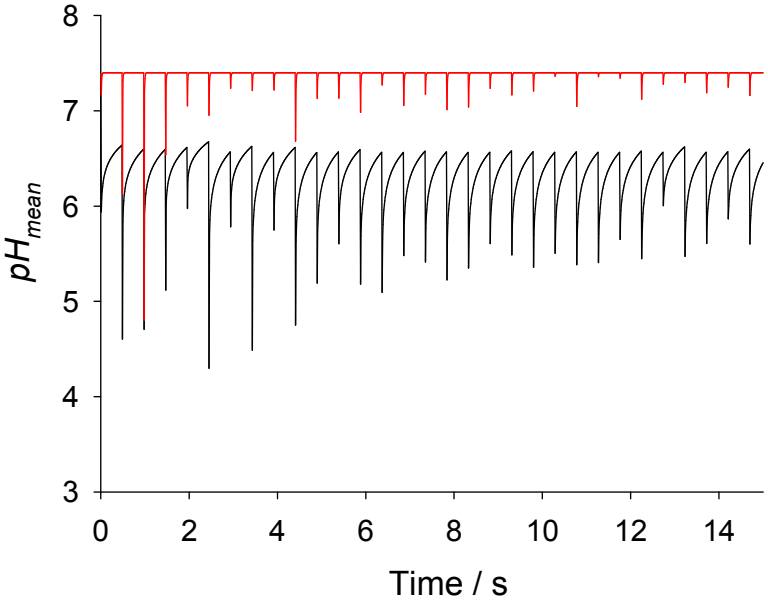
8
7
6
5
4
3
pH_{mean}
0
2
4
6
8
10
12
14
Time / s

B)

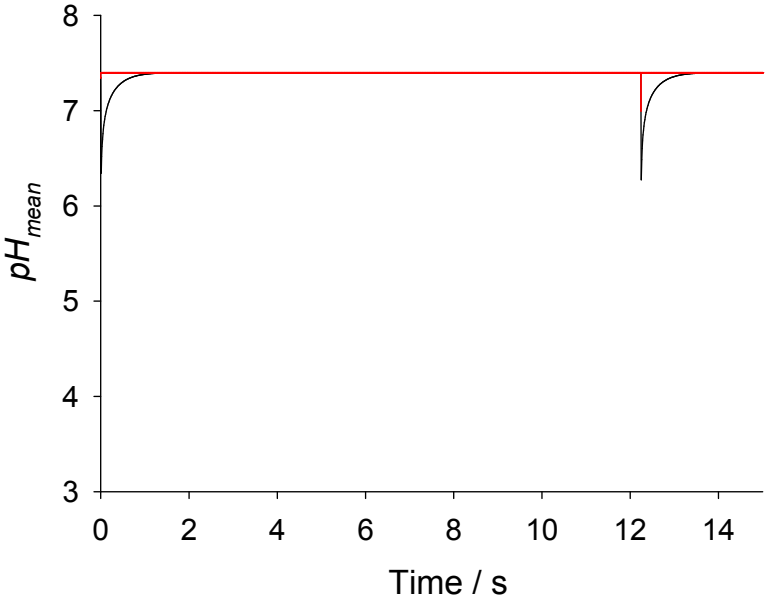
8
7
6
5
4
3
pH_{mean}
0
2
4
6
8
10
12
14
Time / s

C)

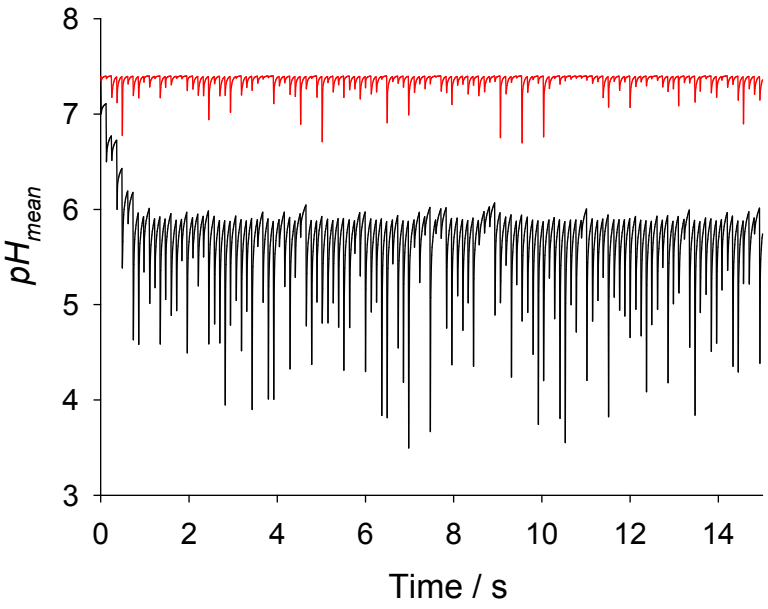

Figure 5

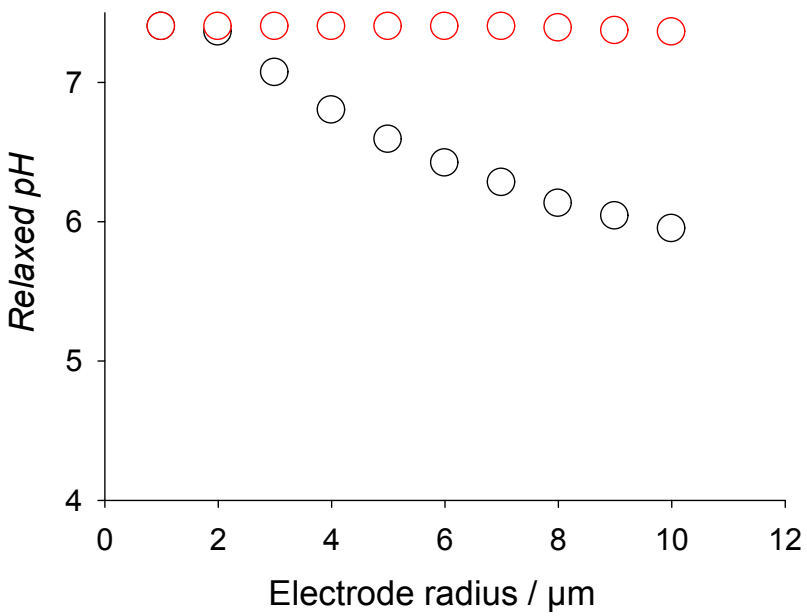

Figure 6

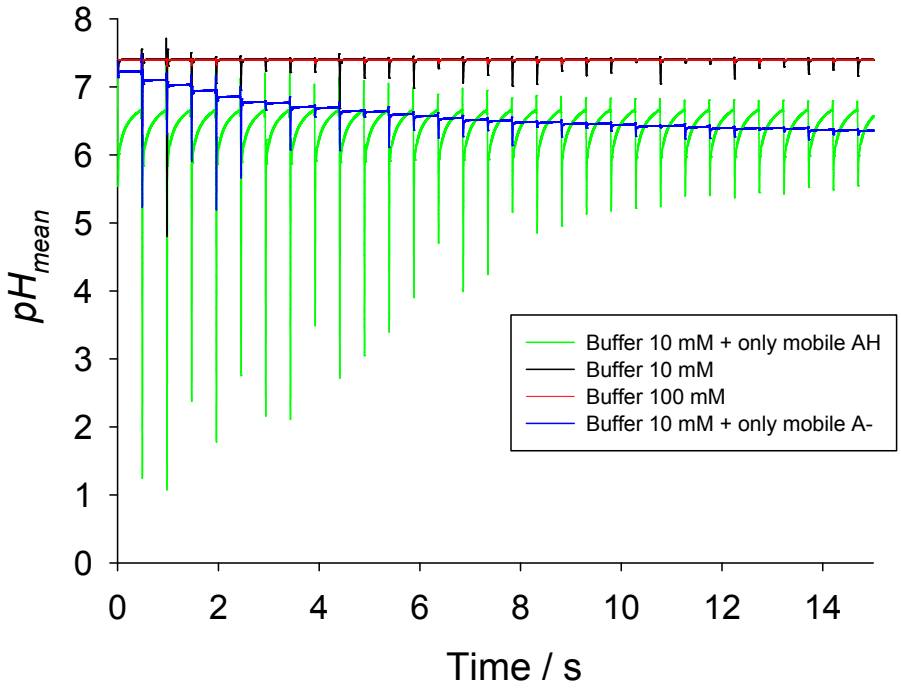

REFERENCES

[1] R. D. Burgoyne, A. Morgan *Physiol. Rev.* **2003**, *83*, 581-632.

[2] R. Borges, N. Dominguez, J. Estevez-Herrera, D. Pereda, J. David Machado *Cell Calcium*. **2012**, *51*, 338-341.

[3] T. C. Suedhof, J. Rizo *Cold Spring Harb. Perspect. Biol.* **2011**, *3*, a005637.

[4] E. R. Travis, R. M. Wightman *Annu. Rev. Biophys. Biomol. Struct.* **1998**, *27*, 77-103.

[5] E. S. Bucher, R. M. Wightman *Annu. Rev. Anal. Chem.* **2015**, *8*, 239-261.

[6] C. Amatore, S. Arbault, M. Guille, F. Lemaitre *Chem. Rev.* **2008**, *108*, 2585-2621.

[7] H. Fathali, A.-S. Cans *Pflügers Arch.* **2018**, *470*, 125-134.

[8] M. Shin, Y. Wang, J. R. Borgus, B. J. Venton *Annu. Rev. Anal. Chem.* **2019**, *12*, 297-321.

[9] X. Liu, Y. Tong, P.-P. Fang *Trends Anal. Chem.* **2019**, *113*, 13-24.

[10] L. Ren, L. J. Mellander, J. Keighron, A.-S. Cans, M. E. Kurczy, I. Svir, A. Oleinick, C. Amatore, A. G. Ewing *Q. Rev. Biophys.* **2016**, *49*, e12.

[11] Y. Wang, A. Ewing *ChemBioChem*. **2021**, *22*, 807-813.

[12] N. T. N. Phan, X. Li, A. G. Ewing *Nat. Rev. Chem.* **2017**, *1*, 0048.

[13] A. Oleinick, F. Lemaitre, M. G. Collignon, I. Svir, C. Amatore *Faraday Discuss.* **2013**, *164*, 33-55.

[14] S. Ge, S. Koseoglu, C. L. Haynes *Anal. Bioanal. Chem.* **2010**, *397*, 3281-3304.

[15] J. D. Keighron, A. G. Ewing, A.-S. Cans *Analyst*. **2012**, *137*, 1755-1763.

[16] J. D. Keighron, Y. Wang, A.-S. Cans *Annu. Rev. Anal. Chem.* **2020**, *13*, 159-181.

[17] D. M. Omiatek, A.-S. Cans, M. L. Heien, A. G. Ewing *Anal. Bioanal. Chem.* **2010**, *397*, 3269-3279.

[18] R. Borges, M. Camacho, K. D. Gillis *Acta Physiol.* **2008**, *192*, 173-184.

[19] Y. Liu, J. Du, M. Wang, J. Zhang, C. Liu, X. Li *Front. Chem.* **2021**, *8*, 591311.

[20] Y.-T. Li, S.-H. Zhang, X.-Y. Wang, X.-W. Zhang, A. I. Oleinick, I. Svir, C. Amatore, W.-H. Huang *Angew. Chem., Int. Ed. Engl.* **2015**, *54*, 9313-9318.

[21] S. Majdi, E. C. Berglund, J. Dunevall, A. I. Oleinick, C. Amatore, D. E. Krantz, A. G. Ewing *Angew. Chem., Int. Ed. Engl.* **2015**, *54*, 13609-13612.

[22] Y. Tang, X.-K. Yang, X. Zhang, W.-T. Wu, F.-L. Zhang, H. Jiang, Y.-L. Liu, C. Amatore, W.-H. Huang *Chem. Sci.* **2020**, *11*, 778-785.

[23] C. Amatore, S. Arbault, Y. Bouret, M. Guille, F. Lemaitre, Y. Verchier *Anal. Chem.* **2009**, *81*, 3087-3093.

[24] E. V. Mosharov, D. Sulzer *Nat. Methods*. **2005**, *2*, 651-658.

[25] M. Guille-Collignon, F. Lemaitre *Trends Anal. Chem.* **2020**, *132*, 116055.

[26] X. Liu, L. Hu, N. Pan, L. Grimaud, E. Labbe, O. Buriez, J. Delacotte, F. Lemaitre, M. Guille-Collignon *Biophys. Chem.* **2018**, *235*, 48-55.

[27] X. Liu, A. Savy, S. Maurin, L. Grimaud, F. Darchen, D. Quinton, E. Labbe, O. Buriez, J. Delacotte, F. Lemaitre, M. Guille-Collignon *Angew. Chem., Int. Ed. Engl.* **2017**, *56*, 2366-2370.

[28] A. Meunier, O. Jouannot, R. Fulcrand, I. Fanget, M. Bretou, E. Karatekin, S. Arbault, M. Guille, F. Darchen, F. Lemaitre, C. Amatore *Angew. Chem., Int. Ed. Engl.* **2011**, *50*, 5081-5084.

[29] C. Amatore, S. Arbault, Y. Bouret, M. Guille, F. Lemaitre *ChemPhysChem*. **2010**, *11*, 2931-2941.

[30] S.-H. Chen, A. Chao, C.-L. Tsai, S.-C. Sue, C.-Y. Lin, Y.-Z. Lee, Y.-L. Hung, A.-S. Chao, A.-J. Cheng, H.-S. Wang, T.-H. Wang *Mol. Ther. Methods Clin. Dev.* **2019**, *13*, 99-111.

[31] S. M. Saparov, Y. N. Antonenko, P. Pohl *Biophys. J.* **2006**, *90*, L86-L88.

[32] C. A. Aspinwall, S. A. Brooks, R. T. Kennedy, J. R. T. Lakey *J. Biol. Chem.* **1997**, *272*, 31308-31314.

[33] M. D. Hawley, S. V. Tatawawa, S. Piekarsk, R. N. Adams *J. Am. Chem. Soc.* **1967**, *89*, 447-450.

[34] J. A. Jankowski, J. M. Finnegan, R. M. Wightman *J. Neurochem.* **1994**, *63*, 1739-1747.

[35] J. A. Jankowski, T. J. Schroeder, E. L. Ciolkowski, R. M. Wightman *J. Biol. Chem.* **1993**, *268*, 14694-14700.

[36] R. T. Kennedy, H. A. Lan, C. A. Aspinwall *J. Am. Chem. Soc.* **1996**, *118*, 1795-1796.

[37] S. C. Taylor, M. L. Roberts, C. Peers *J. Physiol. (Lond.)*. **1999**, *519*, 765-774.

[38] Y. Bouret, M. Argentina, L. Counillon *Plos One*. **2014**, *9*, e85449.

[39] L. Counillon, Y. Bouret, I. Marchiq, J. Pouyssegur *Biochim. Biophys. Acta, Mol. Cell Res.* **2016**, *1863*, 2465-2480.

[40] C. Amatore, S. Arbault, I. Bonifas, F. Lemaitre, Y. Verchier *ChemPhysChem*. **2007**, *8*, 578-585.

[41] C. Amatore, S. Arbault, Y. Bouret, M. Guille, F. Lemaitre, Y. Verchier *ChemBioChem*. **2006**, *7*, 1998-2003.